RAA 2015 Vol. **15** No. **9**, 1455–1466 doi: 10.1088/1674–4527/15/9/002
http://www.raa-journal.org *http://www.iop.org/journals/raa*

Research in Astronomy and Astrophysics

The nature of the γ-ray flare associated with blazar 3C 454.3

Wen Hu, Zhong-Hui Fan and Ben-Zhong Dai*

[1] Department of Astronomy, Yunnan University, Kunming 650091, China; *bzhdai@ynu.edu.cn*
[2] Key Laboratory of Astroparticle Physics, Yunnan Province, Kunming 650091, China

Received 2014 September 24; accepted 2015 January 31

Abstract We have studied the simultaneous spectral energy distributions (SEDs) of the 2009 December flare and those of the quiescent state of *blazar 3C 454.3* by constructing a multi-component model. We find that all six SEDs can be explained by a one-zone leptonic model involving synchrotron self-Compton (SSC) plus external Compton emission from an accretion disk (ECD) and that from a broad-line region (ECC). X-ray emission is dominated by the SSC mechanism, and the γ-ray spectrum is well represented by a combination of ECD and ECC processes. Our results indicate that the energy density of the magnetic field and electrons decrease with distance from the central engine, and the Doppler factor increases with the blob moving outward in the development of the 2009 December flare. The increase in the observed flux density is possibly due to the increase in the Doppler factor of the blob. The relation between the Doppler factor $\delta_{\rm b}$ and the distance from the central black hole suggests the magnetically driven jets span a sub-pc scale, and the relation between the magnetic field B' and the dimension of the emission region $R'_{\rm b}$ is in good agreement with what is required by conservation of magnetic flux. The weak "harder-when-brighter" behavior of the γ-ray spectrum could be a result of the increase in Doppler factor during the outward motion of the blob. The parameters during the quiescent state obviously deviate from those during the flare state. We propose that the flare was likely caused by the ejection of a new blob. The gamma-ray emissions in different states are associated with the evolution of the blob.

Key words: radiation mechanisms: non-thermal — methods: numerical — galaxies: active — quasars: individual (3C 454.3)

1 INTRODUCTION

Blazars include flat-spectrum radio-loud quasars (FSRQs) and BL Lac objects with relativistic jets pointed closed to our line of sight, and can be detected with strong variability from the radio to γ-ray bands. In general, the non-thermal emission from blazars originates in relativistic jets that are beamed and Doppler-boosted towards the observer. The broadband spectral energy distribution (SED) of blazars typically exhibits a double-peaked structure. It is commonly accepted that the low-energy component spanning the range from radio to ultraviolet (UV) bands, sometimes extending to the X-ray band, is interpreted as synchrotron emission. The high-energy component located at γ-ray energies may be attributed to inverse Compton up-scattering off internal synchrotron photons of the

* Corresponding author

same electron population (synchrotron self-Compton model (SSC), Bloom & Marscher 1996; Finke et al. 2008), or the external radiation field intercepted by the jet (external Compton model (EC)). The external photon field includes photons directly from the accretion disk surrounding the black hole (BH) in the center of an active galaxy (Dermer & Schlickeiser 2002), the radiation reprocessed and scattered by clouds in a broad line region (BLR) (Dermer et al. 2009), and the infrared (IR) emission from the dusty torus (Sikora et al. 1994).

3C 454.3 is one of the most remarkable blazars at redshift $z = 0.859$ (Jackson & Browne 1991). Since 2000, the source has been exhibiting exceptionally active behavior from radio to the very high energy (VHE) γ-ray bands (Vercellone et al. 2008; Donnarumma et al. 2009; Ackermann et al. 2010; Abdo et al. 2011). The rapid and violent variability, most notably in the γ-ray band, is still poorly understood. In order to interpret the variability characteristics at different frequencies, an interpretation involving changes in the viewing angle of the different emitting regions of the jet with respect to the line of sight has been proposed by some authors (Villata et al. 2007; Raiteri et al. 2008a,b). Ghisellini et al. (2007) constructed simultaneous SEDs covering the radio to γ-ray bands in 2000, 2005 and 2007 but obtained poor results in the γ-ray band, and found that the SEDs can be reproduced by Katarzyński & Ghisellini (2007) who invoked an internal shock scenario in which the jet power is assumed to be constant. The idea of a constant jet power might be challenged when the γ-ray band has been detected by *AGILE* and *Fermi*, because a real increase of the jet power is flagged by the increased emissions in the optical and γ-ray bands (Ghisellini et al. 2007). By analyzing the behavior of the parsec-scale jet of 3C 454.3, Jorstad et al. (2010) concluded that the three major flares may be associated with propagating disturbances, and suggested that the location of the dissipation region of the 2005 May flare may be closer to the central BH. Bonnoli et al. (2011) found that a simple one-zone SSC-plus-EC model can account for all the considered SEDs, and suggested that the flare could be due to the injection of electrons based on the results from independent fits of the SEDs at six different epochs. The other surprising result is that the GeV γ-ray spectra are much better described by a broken power law than by a simple power law or any models that incorporate smooth curves. To date, the origin of the GeV spectral break is still under debate (Abdo et al. 2009; Finke & Dermer 2010; Poutanen & Stern 2010; Stern & Poutanen 2011; Harris et al. 2012; Cerruti et al. 2013). In our model fits, we modeled the GeV γ-ray spectra with a superposition of two different Compton-scattered components (Finke & Dermer 2010; Cerruti et al. 2013).

In this work, we use a simple one-zone model to assess whether or not a flare could be caused by an emission region's outward movement along the jet. In order to determine the physical parameters of the model, we utilize a χ^2 minimization technique in our work. The simultaneous multiwavelength (MWL) data, collected from 2009 November 6 to December 3 (Bonnoli et al. 2011), are used to analyze the nature of the flare associated with blazar 3C 454.3. The giant flare lasted about one month at all wavelengths, and the flux in the γ-ray band reached a peak value of $21.8 \pm 1.2 \times 10^{-6}\ \mathrm{photons\ cm^{-2}\ s^{-1}}$, corresponding to a peak luminosity of $L_\gamma \sim 3 \times 10^{49}\ \mathrm{erg\ s^{-1}}$, a factor of ~ 30 larger than the *EGRET* luminosity. This paper is organized as follows. In Section 2, we describe our model and assumptions; the results of our calculations are presented in Section 3; finally in Section 4, we discuss our results and draw conclusions. In this work, a flat ΛCDM cosmology with $H_0 = 70\ \mathrm{km\ s^{-1}}$, $\Omega_m = 0.3$ and $\Omega_\Lambda = 0.7$ is used.

2 THE MODEL

We adopt a standard one-zone leptonic model to reproduce the simultaneous MWL SEDs at the different states of the 2009 December flare and quiescent state. Studies by some authors have indicated that the differing behaviors of the radio and optical continuum lack correlation, and higher-frequency variations lead to lower-frequency ones in the radio band (e.g., Villata et al. 2007; Raiteri et al. 2011; Ogle et al. 2011). However, the γ-ray emission has been observed to correlate with the optical and X-ray bands, supporting a single emission zone, with no significant lag between optical and γ-rays

(Bonning et al. 2009; Bonnoli et al. 2011). For simplicity, the emission zone is assumed to be a blob of radius $R'_{\rm b} = c\delta_b t_{\rm var}/(1+z)$ in the comoving frame, which moves with a Lorentz factor $\Gamma_{\rm b}$ at an angle $\theta_{\rm obs}$ with respect to the line of sight. $t_{\rm var}$ is the γ-ray light variability time and z is the source redshift. $\delta_{\rm b} = [\Gamma_{\rm b}(1-\beta_{\rm b}\cos\theta_{\rm b})]^{-1}$ is the blob's Doppler factor, where $\beta_{\rm b}$ is the blob's speed in units of the speed of light. In the comoving frame of the blob, the magnetic field is assumed to be randomly oriented, and the relativistic electron distribution is assumed to be isotropic (Dermer et al. 2009; Band et al. 1993),

$$\begin{aligned} n'_{\rm e}(\gamma') \;=\; & K'_{\rm e} H(\gamma';\gamma'_{\rm min},\gamma'_{\rm max})\Big\{\gamma'^{-p_1}\exp(-\gamma'/\gamma'_{\rm b}) \\ & \times H[(p_2-p_1)\gamma'_{\rm b}-\gamma'] + [(p_2-p_1)\gamma'_{\rm b}]^{p_2-p_1} \\ & \times \gamma'^{-p_2}\exp(p_1-p_2)H[\gamma'-(p_2-p_1)\gamma'_{\rm b}]\Big\}, \end{aligned} \tag{1}$$

where $K'_{\rm e}$ is the normalization factor, and p_1 and p_2 are spectral indices of the pre- and post-break Lorentz factor $\gamma'_{\rm b}$, respectively, and where $\gamma'_{\rm min}$ and $\gamma'_{\rm max}$ are the low energy and high energy cut-offs, respectively. $H(x;x_1,x_2)$ and $H(x)$ are the two versions of the Heaviside function: $H(x;x_1,x_2)=1$ for $x_1 \le x \le x_2$ and $H(x;x_1,x_2)=0$ everywhere else, while $H(x)=1$ for $x \ge 0$ and $H(x)=0$ for $x \le 0$.

In the model, photons from the accretion disk and from the BLR are considered (Foschini et al. 2010; Tavecchio et al. 2010; Yan et al. 2013). These photons were detected during faint states of the source (Raiteri et al. 2007; Ikejiri et al. 2011). The accretion disk spectrum is assumed to be a Shakura & Sunyaev (1973) disk spectrum extending from $6R_{\rm g}$ to $5000R_{\rm g}$, and its luminosity is also assumed to be constant. The angular dependent energy density directed away from the accretion disk at position $z_{\rm b}$ is

$$u_{*,\rm DISK}(\epsilon_*,\Omega_*) = \frac{2m_{\rm e}c^2}{\lambda_{\rm C}^3}\frac{\epsilon_*^3}{\exp(\epsilon_*/\Theta(\tilde{R}))-1}, \tag{2}$$

where $\lambda_{\rm C} = h/m_{\rm e}c$ is the Compton wavelength of the electron. $\Theta(\tilde{R}) = \frac{k_{\rm B}T(\tilde{R})}{m_{\rm e}c^2}$ is the dimensionless temperature of the blackbody radiation field at radius $\tilde{R} = z_{\rm b}\sqrt{\mu_*^{-2}-1}/R_{\rm g}$ in units of gravitational radii $R_{\rm g}$ and $k_{\rm B}$ is Boltzmann's constant. $T(\tilde{R}) = [3L_{\rm d}(1-\sqrt{6/\tilde{R}})/8\pi\eta\sigma_{SB}R_{\rm g}^2\tilde{R}^3]^{1/4}$ is the temperature at radius $\tilde{R}$ for a Schwarzschild metric, where $L_{\rm d}$ is the bolometric luminosity of the accretion disk, $\eta = 1/12$ is the efficiency of transforming accreted matter to escaping radiant energy, and $\sigma_{SB} = 5.6704\times10^{-5}\ {\rm erg\ cm^{-2}\ s^{-1}\ K^{-4}}$ is the Stefan-Boltzmann constant (Dermer & Schlickeiser 2002). In order to model the BLR and its radiation field, we adopt the simplest thin shell model outlined by Donea & Protheroe (2003). For simplicity, we only consider the inverse Compton scattering of the Lyα photons with energy $E_{{\rm Ly}\alpha} \sim 10$ eV, which was observed by the *GALEX* satellite in 2008 October (Bonnoli et al. 2011) and is expected to be much brighter than the other emissions and than the Balmer continuum from the BLR (e.g., $\rm C_{IV}$, $\rm Mg_{II}$, Hα, Hβ, etc) (Francis et al. 1991; Gaskell et al. 1981; Liu & Bai 2006).

In the model, the radius of the BLR, $R_{\rm BLR}$, is far greater than the thickness of the thin spherical shell, $h_{\rm BLR} = R_{\rm o} - R_{\rm i}$, where $R_{\rm o} = R_{\rm BLR} + h_{\rm BLR}/2$ and $R_{\rm i} = R_{\rm BLR} - h_{\rm BLR}/2$ are the outer radius and the inner radius, respectively. Between the inner and outer radius of the BLR, the number density and the radius of clouds are assumed to follow a power-law distribution, for which we adopted the power-law exponents preferred by Kaspi & Netzer (1999): $p = 1.5$ and $q = 1/3$. Then the emission line emissivity is a function of radius r, $j(r) = \frac{(2q-p+1)f_{\rm cov}L_{\rm d}r^{2q-p-2}}{16\pi^2(R_{\rm o}^{2q-p+1}-R_{\rm i}^{2q-p+1})}$, where $f_{\rm cov}$ is the covering factor for the entire BLR associated with the central UV radiation. The energy density of the BLR photons at angle $\theta = \arccos\mu_*$ with respect to the jet axis at position $z_{\rm b}$ is

$$u_{*,\ \rm BLR}(z_{\rm b},\mu_*) = \int_0^{\ell_{\rm min1}} d\ell j(r)/c + \int_{\ell_{\rm min2}}^{\ell_{\rm max}} d\ell\ j(r)/c\,, \tag{3}$$

where

$$r^2 = z_{\rm b}^2 - 2z_{\rm b}\ell\mu_* + \ell^2\,, \tag{4}$$

$$\ell_{\rm min1,2} = z_{\rm b}\mu_* \pm z_{\rm b}\sqrt{\mu_*^2 + (R_{\rm i}/z_{\rm b})^2 - 1}\,, \tag{5}$$

$$\ell_{\rm max} = z_{\rm b}\mu_* + z_{\rm b}\sqrt{\mu_*^2 + (R_{\rm o}/z_{\rm b})^2 - 1}\,. \tag{6}$$

The luminosity of the accretion disk and the BLR can be estimated from observations, thus the radius of the BLR is the only essential parameter describing the external photon field that we consider. Note that throughout this paper, unprimed quantities refer to the observer's frame and primed quantities refer to the comoving frame. We do not consider the absorption of high-energy γ-ray photons due to the pair-production process from extragalactic background light (EBL) or the external photons originating from the accretion disk or BLR in this work (Abdo et al. 2009; Anderhub et al. 2009; Finke et al. 2010; Finke & Dermer 2010).

The observed flux density is given by

$$\nu F_\nu^{\rm SYN} = \frac{\pi R_{\rm b}^2}{4\pi d_L^2}\delta_{\rm b}^4\epsilon' I'(\epsilon')\,, \tag{7}$$

where d_L is the luminosity distance and $I'(\epsilon') = \frac{j'_s(\epsilon')}{\kappa'(\epsilon')}[1-\exp(-\kappa'(\epsilon')R'_{\rm b})]$ is the synchrotron intensity that is assumed to be uniform for a spherical geometry. The synchrotron radiation coefficient and the absorption coefficient for isotropic relativistic electrons in a randomly oriented magnetic field are respectively given by

$$j'_s(\epsilon') = \int_{\gamma'_{\rm min}}^{\gamma'_{\rm max}} n'_{\rm e}(\gamma')P'_{\rm e}(\epsilon',\gamma')d\gamma'\,, \tag{8}$$

$$\kappa'(\epsilon') = -\frac{h^3}{8\pi m_{\rm e}^4 c^6 \epsilon'^2}\int_{\gamma'_{\rm min}}^{\gamma'_{\rm max}}\frac{d}{d\gamma'}\left[\frac{n'_{\rm e}(\gamma')}{\gamma'^2}\right]\gamma'^2 P'_{\rm e}(\epsilon',\gamma')d\gamma'\,. \tag{9}$$

Here $P'_{\rm e}(\epsilon',\gamma') = \frac{\sqrt{3}e^3B'}{h}R(x)$ is the mean emission coefficient for a single electron integrated over the isotropic distribution of pitch angles in which e is the electron charge and h is the Planck constant (Blumenthal & Gould 1970). In our calculation we use an approximation for $R(x)$ presented by Finke et al. (2008) where $x = 4\pi\epsilon' m_{\rm e}^2c^3/(3eB'h\gamma'^2)$. $\epsilon' m_{\rm e}c^2 = h\nu\delta_{\rm b}/(1+z)$ is the synchrotron photon energy, where ν is the observed frequency.

The SSC flux density is given by Finke et al. (2008),

$$\begin{aligned}\nu F_\nu^{SSC} &= \frac{3c\sigma_{\rm T}{\epsilon'_s}^2\delta_{\rm b}^4 V'_{\rm b}}{16\pi d_L^2}\int_0^\infty d\epsilon'\frac{u'_{\rm syn}(\epsilon')}{\epsilon'^2} \\ &\quad\times\int_{\gamma'_{\rm min}}^{\gamma'_{\rm max}}d\gamma'\frac{n'_{\rm e}(\gamma')}{\gamma'^2}F_{\rm C}(q,\Gamma_{\rm e}),\end{aligned} \tag{10}$$

where $\sigma_{\rm T}$ is the Thomson cross section and $u'_{\rm syn}(\epsilon') = 0.75\cdot I'(\epsilon')/c$ is the field energy density of synchrotron radiation over the solid angle (Gould 1979). $V'_{\rm b} = 4\pi {R'_{\rm b}}^3/3$ is the blob's comoving volume. $\epsilon'_s m_{\rm e}c^2 = h\nu\delta_{\rm b}/(1+z)$ is the self-Compton scattered photon energy, where ν is the observed frequency. The inverse-Compton core $F_{\rm C}(q,\Gamma_{\rm e}) = 2q\ln q + (1+2q)(1-q) + \frac{q^2\Gamma_{\rm e}^2(1-q)}{2(1+q\Gamma_{\rm e})}$, where $q = \frac{\epsilon'/\gamma'}{\Gamma_{\rm e}(1-\epsilon/\gamma')}$ is in the range $[\frac{1}{4\gamma'^2},1]$ and $\Gamma_{\rm e} = 4\epsilon'\gamma'$.

The observed Compton-scattered external photon field spectra can be calculated from the following formula,

$$\nu F_{\nu}^{EC} = \frac{3c\sigma_{\rm T}{\epsilon_s}^2\delta_{\rm b}^3 V'_{\rm b}}{32\pi d_L^2}\oint d\Omega_* \int_0^{\infty} d\epsilon_* \frac{u_*(\epsilon_*,\Omega_*)}{\epsilon_*^2} \times \int_{\gamma'_{\rm min}\delta_{\rm b}}^{\gamma'_{\rm max}\delta_{\rm b}} d\gamma \frac{n'_{\rm e}(\gamma/\delta)}{\gamma^2}\Xi H\Big(\epsilon_s;\frac{\overline{\epsilon}}{2\gamma},\frac{2\gamma\overline{\epsilon}}{1+2\overline{\epsilon}}\Big), \quad (11)$$

where $\Xi \equiv y + y^{-1} - \frac{2\epsilon_s}{\gamma\overline{\epsilon}y} + (\frac{\epsilon_s}{\gamma\overline{\epsilon}y})^2$, $y \equiv 1 - \frac{\epsilon_s}{\gamma}$ and the invariant collision energy $\overline{\epsilon} \simeq \gamma\epsilon_*(1-\sqrt{1-1/\gamma^2}\mu_*)$. $\epsilon_s m_{\rm e}c^2 = h\nu(1+z)$ is the Compton-scattered photon energy where ν is the observed frequency. The density of target photons $u_*(\epsilon_*,\Omega_*)$ is calculated by Equations (2) and (3).

3 RESULTS

The simultaneous MWL SEDs of blazar 3C 454.3 obtained by Bonnoli et al. (2011) are used to analyze the development of the flare observed in 2009 November-December. The following constraints on the parameters are from the observations and the results of other authors:

(1) The variability timescale is assumed to be on the order of several hours (Tavecchio et al. 2010; Foschini et al. 2010).
(2) The beaming effect plays an important role in the high luminosity and rapid variability detected in γ-ray loud blazars. Unfortunately, both the Lorentz factor and the viewing angle are unobservable. Different methods have been used to estimate the Doppler factor by many authors (e.g., Mattox et al. 1993; Lähteenmäki & Valtaoja 1999; Zhang et al. 2002; Xiang & Dai 2007, etc). In this work, the minimum Doppler factor $\delta_{\rm min} \sim 13$ and the upper limit of the Doppler factor $\delta_{\rm b} \sim 25$ are adopted, which were derived from the flux variability time and highest energy photon measurements (Ackermann et al. 2010), and from the long-term very long baseline interferometry (VLBI) (Jorstad et al. 2005; Lister et al. 2009), respectively.
(3) Following the analysis of the estimate of BH mass by Bonnoli et al. (2011), the mass of the BH is assumed to be $5\times10^8 M_{\odot}$. The bolometric luminosity of the accretion disk surrounding the central BH, $L_{\rm d} \sim 3\times10^{46}$ erg s^{-1}, is adopted (Raiteri et al. 2007). The BLR luminosity is assumed to be $L_{\rm BLR} \sim 3\times10^{45}$ erg s^{-1} (Pian et al. 2005, 2006), which implies a typical covering factor of $f_{\rm cov} \sim 10\%$. The accretion disk and BLR luminosity are derived when the source is in a faint state.

In order to avoid $\gamma\gamma$ absorption by interaction with the photons originating from the BLR, the BLR is assumed to be located at $R_{\rm BLR} = 9\times10^{17}$ cm when the GeV γ-ray radiation is produced at the smallest allowed distance of 10^{-2} pc from the central BH (Ghisellini & Madau 1996). For the purpose of illustration, the left panel of Figure 1 shows the relationship between the energy density of BLR-reprocessed radiation with different $R_{\rm BLR}$ and $h_{\rm BLR}$ for the BLR structure and the location of the emission region, while we show the $\gamma\gamma$ absorption optical depth, $\tau_{\gamma\gamma}$, due to interactions with Lyα line photons, $\rm He_{II}$ at 54.4 eV and $\rm H_I$ LyC at 13.6 eV from BLR and UV photons from the accretion disk in the right panel of Figure 1. In the left panel of Figure 1, it can be found that the energy density inside the inner radius increases as parameter $h_{\rm BLR}$ increases for a fixed $R_{\rm BLR}$, and increases as the parameter $R_{\rm BLR}$ decreases for a fixed $h_{\rm BLR}$, and vice versa. When considering the above and for simplicity, we assume that a BLR has a thin spherical structure where the details of the radial distribution of the BLR material do not play an important role. If the GeV γ-ray radiation produced at distances $\gtrsim 0.01$ pc can escape from the BLR, the minimum radius of the BLR may be roughly 9×10^{17} cm. Here, the luminosities in $\rm H_I$ LyC at 13.6 eV and

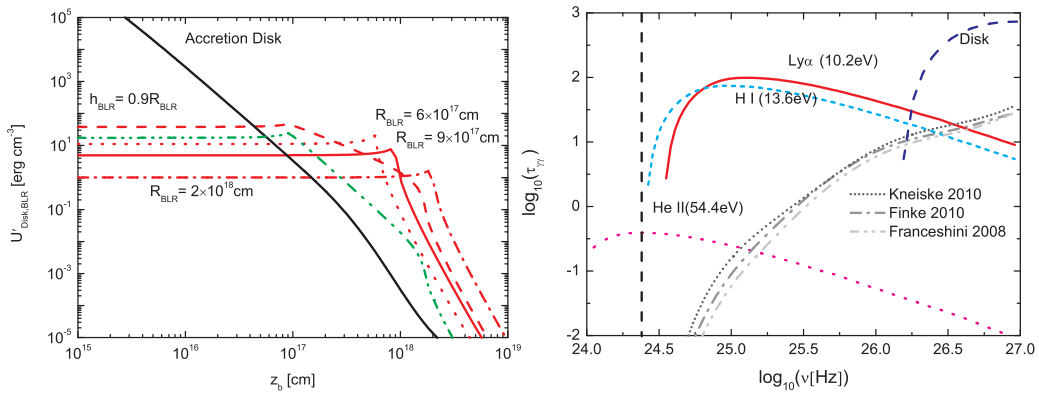

Fig. 1 *Left panel*: the radial dependence of the energy density of the BLR-reprocessed radiation on two parameters $R_{\rm BLR}$ and $h_{\rm BLR}$ in the comoving frame of the emission region with $\Gamma_{\rm b} = 20$. The red solid line labeled by $R_{\rm BLR} = 9 \times 10^{17}$ cm shows the BLR-reprocessed radiation. The dashed, dotted and dash-dotted lines are plotted with different parameters $H_{\rm BLR} = 0.9R_{\rm BLR}$, $R_{\rm BLR} = 6 \times 10^{17}$ cm and $R_{\rm BLR} = 2 \times 10^{18}$ cm, respectively. For a comparison, the energy density directed from the accretion disk and from BLR-scattered radiation is plotted in the figure. The black solid line shows the energy density directed from the accretion disk. The green dash-dot-dotted line shows the energy density directed from BLR-scattered radiation calculated with a wind-like model, where the Thomson scattering depth $\tau_{\rm T} = 0.01$ and the half-thickness $h_{\rm BLR} = 0.9R_{\rm BLR}$ are adopted. *Right panel*: The photoabsorption optical depth of the interaction of the γ-ray photons with the external radiation field. The opacity of the γ-ray photons by the photon-photon pair production on the $\rm Ly\alpha$, $\rm He_{II}$ and $\rm H_I$ line photons from the BLR, and UV photons from the accretion disk are labeled. The optical depth corresponding to the different EBL models is shown in the legend. The vertical dashed line corresponds to the observed γ-ray photon with a maximum energy of ~ 10 GeV.

$\rm Ly\alpha$ line photons at 10.2 eV are assumed to be equal, and the $\rm He_{II}$ luminosity reported by Wills et al. (1995), $L_{\rm He_{II}} \simeq 6 \times 10^{43}$ erg s^{-1}, is adopted for the case of absorption coming from $\rm He_{II}$. Following the straightforward estimation from eq.(2) of Poutanen & Stern (2010), the maximum opacity $\tau = 0.27$ at energy 7.7 GeV (or 2×10^{24} Hz) is in good agreement with the resulting optical depth obtained by us (right panel of Fig. 1). If the $\rm He_{II}$ LyC luminosity is larger than 10^{44} erg s^{-1}, the γ-ray photons at energies 7.7 GeV will suffer significant absorption, which will rapidly decrease below the peak energy. The remarkable absorption by $\rm H_I$ and $\rm Ly\alpha$ line photons should appear above 2.5×10^{24} Hz (or 10.3 GeV), which is the upper bound for energy of the γ-ray spectrum in this work. The absorption coming from the accretion disk is only seen above the energies 0.5 TeV (or 10^{26} Hz).

Additionally, the opacity due to photoabsorption for a γ-ray photon traveling in the EBL is also calculated and plotted in the right panel of Figure 1, where three EBL models are used (Finke et al. 2010; Franceschini et al. 2008; Kneiske & Dole 2010). Thus, γ-ray absorption via photon-photon pair production on the external photons can be regarded as negligible in this work. Note that the formula for absorption has been presented in Gould & Schréder (1967); Dermer et al. (2009).

In the following, we use the improved Levenberg-Marquardt algorithm (Transtrum & Sethna 2012) to fit the SEDs in six different epochs. The modified algorithm is designed to improve both its convergence speed and robustness to initial parameter guesses, which are likely to be the most useful modifications in a problem with many parameters where the usual Levenberg-Marquardt routine often has difficulties (Transtrum & Sethna 2012).

The fitting results are shown in Figures 2 and 3. The results indicate that the simultaneous MWL SEDs in six different epochs can be well reproduced by our model (Fig. 2), and the SEDs of the γ-

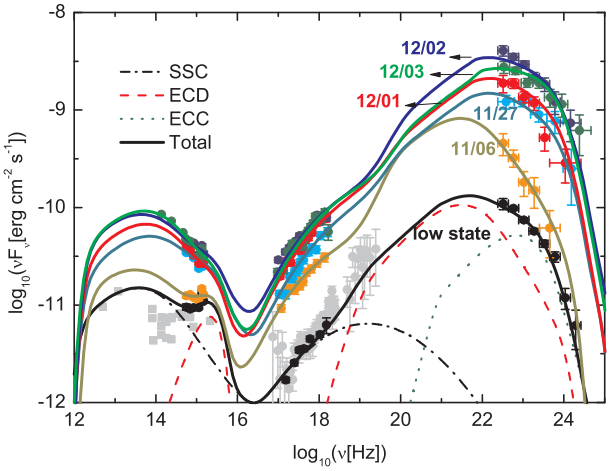

Fig. 2 Multifrequency simultaneous spectra of 3C 454.3 at five different epochs of the 2009 December flare and in the previous quiescent state superimposed on the spectral model. The SEDs in the different epochs are labeled in the figure. The thick solid lines corresponding to the different epochs represent the sum of all the individual components, which contain the accretion disk, the synchrotron, the SSC, the ECD, and the ECC processes. For illustration, individual radiation components of the SED in the quiescent state are shown as dash-dotted lines (synchrotron and SSC), dashed lines (accretion disk and ECD) and dotted lines (ECC). Note that we also show archival data (in gray), including the 2000 June 5–6 *BeppoSAX* data (Tavecchio et al. 2002).

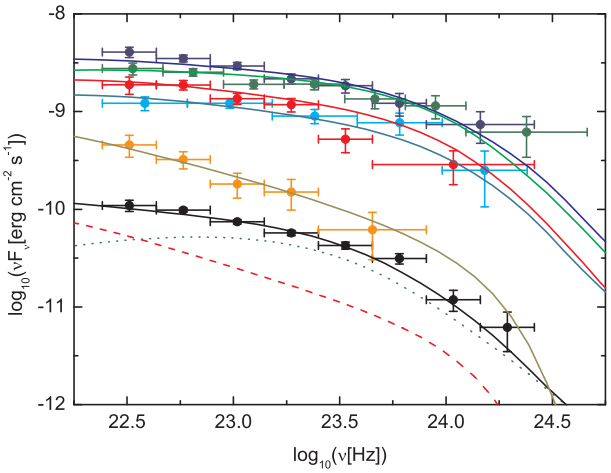

Fig. 3 The modeled γ-ray spectrum compared with the observed data of the γ-ray band.

ray band can be well represented by a combination of external Compton emission from the accretion disk (ECD) and that from the BLR (ECC) (Fig. 3). The input parameters and the ratio of the best fit parameters to the degrees of freedom (dof), Cost/dof, are listed in the upper part of Table 1, where the cost function takes the form $(1/2)\sum_{m=1}^{M}[(f-f_{\rm obs})/\sigma]^2$. In the lower part of Table 1, we list the derived electron energy density ($U'_{\rm e}$) measured in the comoving frame, the radiation efficiency

Table 1 Parameters for the SEDs of 3C 454.3 in the Five Different Epochs and in the Previous Low γ-ray State

	Units	06/11	27/11	01/12	02/12	03/12	Low
$\delta_{\rm b}$		13.8	21.3	23.0	25.2	25.4	17.0
B'		5.98	2.66	2.47	2.34	2.27	4.01
$K'_{\rm e}$	10^5	7.72	2.92	2.63	2.30	1.86	0.64
p_1		1.93	1.86	1.84	1.84	1.83	1.86
p_2		4.11	4.00	4.44	3.93	4.34	4.22
$\gamma'_{\rm min}$		50	50	50	49	58	25
$\gamma'_{\rm b}$		448	746	681	574	633	504
$t_{\rm var}$	h	7.55	6.05	6.01	6.06	6.32	10.0
$z_{\rm b}$	10^{16}	3.04	8.05	8.85	8.98	10.89	7.88
Cost dof		0.74	1.03	1.20	1.98	1.47	1.71
$\lg R'_{\rm b}$		15.78	15.87	15.91	15.95	15.97	15.99
$U'_{\rm e}$		1.57	1.12	1.07	0.87	0.73	0.26
$\lg L_B$		44.97	44.83	44.90	45.01	45.03	45.23
$\lg L_{\rm e}$		45.01	45.43	45.54	45.61	45.58	44.83
$\lg L_{\rm p}$		46.17	46.50	46.62	46.72	46.63	46.17
$\lg L_r$		46.37	46.30	46.38	46.51	46.40	45.48
η		0.58	0.36	0.34	0.36	0.34	0.15

(η) and the power carried by the jet in the form of magnetic field (L_B), cold protons ($L_{\rm p}$), relativistic electrons ($L_{\rm e}$), and produced radiation (L_γ), which are defined by Celotti & Fabian (1993) and Celotti & Ghisellini (2008), and where $\delta_{\rm b} \simeq \Gamma$ is assumed.

We use linear regression to analyze how the Doppler factor $\delta_{\rm b}$ and radiation efficiency η depend on the distance $Z_{\rm b}$, how the magnetic field B' depends on the radius $R'_{\rm b}$, and how the energy density of electrons $U'_{\rm e}$ depends on the product $\Gamma Z_{\rm b}$. The results are plotted in Figure 4, including the best fit and the 95% confidence bands.

We find that there are four good linear relations between the parameters of the flare states in logarithmic space. The relationships of the parameters are: (1) $\delta_{\rm b} \propto Z_{\rm b}^{0.5}$; (2) $\eta \propto Z_{\rm b}^{-0.45}$; (3) $B' \propto {R'_{\rm b}}^{-2.2}$; (4) $U'_{\rm e} \propto (\Gamma Z_{\rm b})^{-0.35}$. The parameter values in the quiescent state are distinct from those in the flare state (see Fig. 4).

4 DISCUSSION AND CONCLUSIONS

In our work, we have studied the flare of blazar 3C 454.3 in 2009 December, which plausibly originated from an emission region propagating in the relativistic jets. By fitting the five simultaneous SEDs of the flare state and one of the quiescent states, we find that (1) all the considered SEDs can be well explained by involving SSC plus the ECD and ECC processes; (2) the power-law index of the relation between B' and $R'_{\rm b}$ is in good agreement with that required for conservation of magnetic flux; (3) the power-law index of the relation between the Doppler factor $\delta_{\rm b}$ and the distance $Z_{\rm b}$ is consistent with what is predicted by magnetically driven jets if we assume the viewing angle $\theta \simeq 1/\delta_{\rm b}$.

The variability of the Doppler factor could be caused by changes in the Lorentz factor (Blandford & Payne 1982; Blandford & Znajek 1977; Li et al. 1992) or the viewing angle of the blob (Qian et al. 1992, 2007, 2014), or even a combination of both. If we assume $\delta_{\rm b} \simeq \Gamma$, an accelerating jet possibly exists at the sub-pc scale where the magnetic driving of the relativistic outflows is supported (Vlahakis & Königl 2004). Alternatively, variation of the Doppler factor along a curved or helical jet is also a possibility. The different behaviors of radio and optical light curves suggest that the optical and radio emissions come from two separate and misaligned jet regions (Villata et al. 2006, 2007). The authors argued that the jet should present some bending. A similar model had been

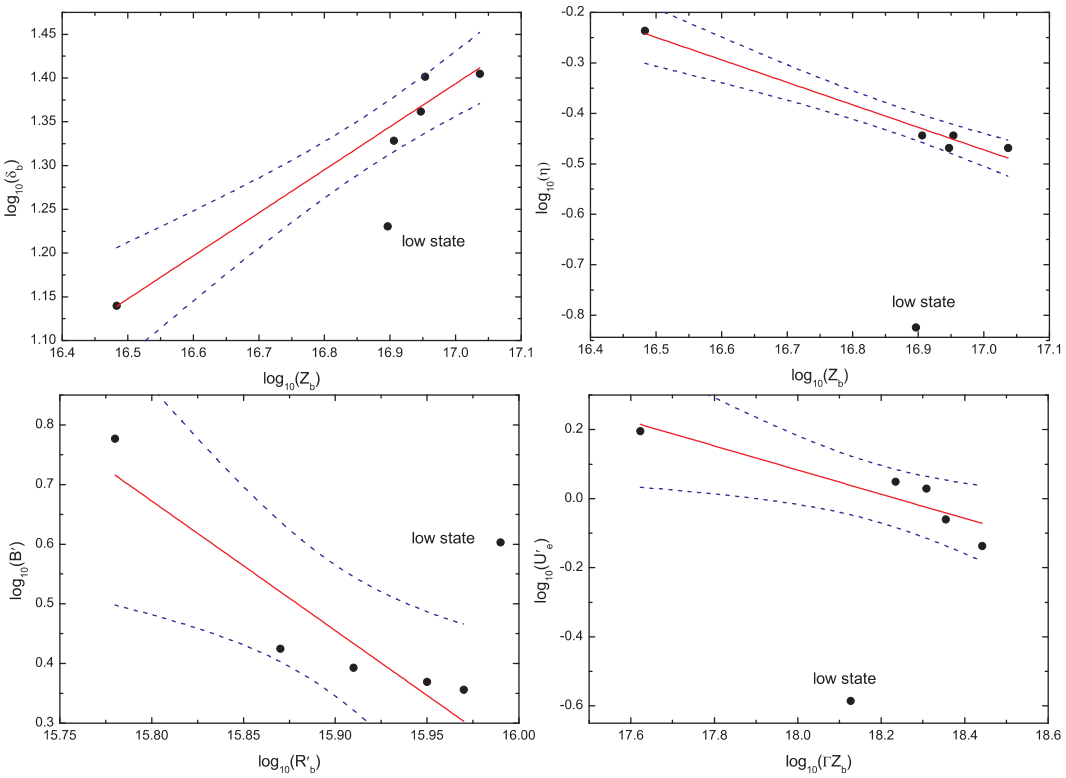

Fig. 4 The linear regression results of parameters for five different SEDs shown in Figure 2. The Doppler factor $\delta_{\rm b}$ and radiation efficiency η as a function of distance are shown in the upper-left and upper-right panels, respectively. The magnetic field B' measured in the comoving frame as a function of the radius of the blob is shown in the lower-left panel. The energy density of electron $U'_{\rm e}$ measured in the comoving frame as the product $\Gamma Z_{\rm b}$ is shown in the lower-right panel. The solid line is the best fit and the dashed curves are the 95% confidence intervals. The corresponding parameters in the low state are also shown in each panel.

adopted to interpret the radio, optical/UV, X-ray and γ-ray behavior from April 2008 to March 2010 (Raiteri et al. 2011). Ogle et al. (2011) presented evidence that the radio-optical SED consists of two variable synchrotron emission peaks, the primary at IR and the secondary at sub-mm wavelengths, likely arising from distinct regions in the jet. The curved-jet motion, with the consequent changes in observation angle, is also supported by the analysis of Britzen et al. (2012), using the VLBI observations of blazar 3C 454.3. The VLBI observations show that the observed accelerations due to significant changes in intrinsic speed and/or direction of features are common, and indicate that changes in the Lorentz factors of features dominate the observed speed changes rather than bends along the line of sight (Lister et al. 2009, 2013; Piner et al. 2012; Homan et al. 2009, 2015). The analysis of Homan et al. (2015) suggests that observed accelerations tend to increase the speed of features near the jet base and decrease their speed at longer distances, and the transition between speeding up and slowing down seems to occur at a projected distance of roughly $\sim 10-20$ pc.

The location of the transition is much farther from the central BH than the location of the blob obtained in our work. The location of the emitting region obtained from the SED modeling is $\sim 0.01-0.1$ pc from the central BH. Our result is in accordance with the general results of some

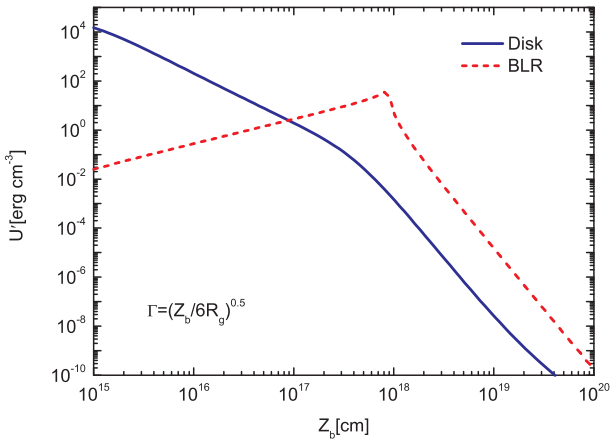

Fig. 5 The change in the energy densities measured in the comoving frame of a magnetically driven jet with the distance from the central BH.

authors through modeling the quasi-simultaneous multifrequency SEDs of the sample from *Fermi* (Ghisellini et al. 2010; Yan et al. 2012), where all the SEDs of FSRQs can be well reproduced when the emission regions lie in the range from several hundred to several thousand Schwarzschild radii from the central BH.

At the different distances from the central BH, the corresponding Doppler factors obtained from the SED modeling vary from 13.8 to 25.4. Ghisellini et al. (2007) modeled the outburst in 2005 as an event that occurred closer to the BH than the outburst in 2007, and the derived Doppler factors are ~ 13 and ~ 16, respectively. Bonnoli et al. (2011) modeled the outburst in 2009, and the derived Doppler factor ranged from 24.5 to 28.5 in different states. The values are smaller than the value of the variable Doppler factors, $\delta_{\rm var} \sim 33$, estimated from radio data (Hovatta et al. 2009; Savolainen et al. 2010). Jorstad et al. (2010) derived the Doppler factors of superluminal knots K1, K2, and K3 as being 23.4, 17.6, and 49.1, respectively. It would mean that the Doppler factor will slowly increase and achieve relatively stable values or decrease when the blob is at a larger distance, which could be determined by the external environment surrounding the jet and the driving mechanism of the jet (Blandford & Payne 1982; Blandford & Znajek 1977). Additionally, the simple relation between the Doppler factor and the distance from the BH possibly implies that the jet has bulk velocity structures. An inhomogeneous jet model with bulk velocity structures is probably more realistic for discussing the multifrequency emissive properties, in which both viewing angles and bulk velocity structures play important roles in the Doppler beaming pattern (Ghisellini et al. 1985; Blandford & Levinson 1995; Yang et al. 2009).

Based on the model fitting and the results of linear correlation of parameters, we propose that the 2009 December flaring event could have given rise to the change in Doppler factor, and that the emission in the flare state likely comes from a new blob propagating along the jet axis. We could infer the physical picture, where blobs are ejected from the base of the jet and move outward along the jet axis, the energy density of the magnetic field and electrons decrease, and the radiation efficiency also decreases, while its radius and the Doppler factor both increase. Compared with the contribution from Compton up-scattering of photons directly from the accretion disk, the contribution of the Comptonization of photons reprocessed by clouds in the BLR gradually increases with distance from the central BH. The increase in the observed flux density could be directly caused by the increase of the Doppler factor, which suggests that there may exist magnetically driven jets in FSRQ 3C 454.3. For illustration, the energy densities of the BLR and of the accretion disk in the comoving frame are

presented in Figure 5, where the bulk Lorentz factor $\Gamma = (Z_{\rm b}/6R_{\rm g})^{0.5}$. Thus, the weakly "harder-when-brighter" behavior of the γ-ray spectrum can be naturally explained. In turn, understanding whether the "harder-when-brighter" behavior of the γ-ray spectrum is an indicator of geometrical motion in the jets of blazar 3C 454.3 will need more detailed observations with more sensitive instruments in the future.

Acknowledgements The authors would like to thank the anonymous referee for his/her constructive comments and suggestions that helped to improve the manuscript. We acknowledge G. Bonnoli for providing the SEDs at the six different epochs and L. Pacciani for the helpful discussion. We acknowledge M. K. Transtrum for using the improved Levenberg-Marquardt algorithm routine. This work was supported by the National Natural Science Foundation of China (Grant Nos. 11063003 and 11463006) and the Graduate Science Foundation of Yunnan University (Grant No. ynuy201262).

References

Abdo, A. A., Ackermann, M., Ajello, M., et al. 2009, ApJ, 699, 817
Abdo, A. A., Ackermann, M., Ajello, M., et al. 2011, ApJ, 733, L26
Ackermann, M., Ajello, M., Baldini, L., et al. 2010, ApJ, 721, 1383
Anderhub, H., Antonelli, L. A., Antoranz, P., et al. 2009, A&A, 498, 83
Band, D., Matteson, J., Ford, L., et al. 1993, ApJ, 413, 281
Blandford, R. D., & Znajek, R. L. 1977, MNRAS, 179, 433
Blandford, R. D., & Payne, D. G. 1982, MNRAS, 199, 883
Blandford, R. D., & Levinson, A. 1995, ApJ, 441, 79
Bloom, S. D., & Marscher, A. P. 1996, ApJ, 461, 657
Blumenthal, G. R., & Gould, R. J. 1970, Reviews of Modern Physics, 42, 237
Bonning, E. W., Bailyn, C., Urry, C. M., et al. 2009, ApJ, 697, L81
Bonnoli, G., Ghisellini, G., Foschini, L., Tavecchio, F., & Ghirlanda, G. 2011, MNRAS, 410, 368
Britzen, S., Zamaninasab, M., Aller, M., et al. 2012, Journal of Physics Conference Series, 372, 012029
Celotti, A., & Fabian, A. C. 1993, MNRAS, 264, 228
Celotti, A., & Ghisellini, G. 2008, MNRAS, 385, 283
Cerruti, M., Dermer, C. D., Lott, B., Boisson, C., & Zech, A. 2013, ApJ, 771, L4
Dermer, C. D., Finke, J. D., Krug, H., & Böttcher, M. 2009, ApJ, 692, 32
Dermer, C. D., & Schlickeiser, R. 2002, ApJ, 575, 667
Donea, A.-C., & Protheroe, R. J. 2003, Astroparticle Physics, 18, 377
Donnarumma, I., Pucella, G., Vittorini, V., et al. 2009, ApJ, 707, 1115
Finke, J. D., & Dermer, C. D. 2010, ApJ, 714, L303
Finke, J. D., Dermer, C. D., & Böttcher, M. 2008, ApJ, 686, 181
Finke, J. D., Razzaque, S., & Dermer, C. D. 2010, ApJ, 712, 238
Foschini, L., Tagliaferri, G., Ghisellini, G., et al. 2010, MNRAS, 408, 448
Franceschini, A., Rodighiero, G., & Vaccari, M. 2008, A&A, 487, 837
Francis, P. J., Hewett, P. C., Foltz, C. B., et al. 1991, ApJ, 373, 465
Gaskell, C. M., Shields, G. A., & Wampler, E. J. 1981, ApJ, 249, 443
Ghisellini, G., Maraschi, L., & Treves, A. 1985, A&A, 146, 204
Ghisellini, G., & Madau, P. 1996, MNRAS, 280, 67
Ghisellini, G., Foschini, L., Tavecchio, F., & Pian, E. 2007, MNRAS, 382, L82
Ghisellini, G., Tavecchio, F., Foschini, L., et al. 2010, MNRAS, 402, 497
Gould, R. J., & Schréder, G. P. 1967, Physical Review, 155, 1404
Gould, R. J. 1979, ApJ, 230, 967
Harris, J., Daniel, M. K., & Chadwick, P. M. 2012, ApJ, 761, 2
Homan, D. C., Kadler, M., Kellermann, K. I., et al. 2009, ApJ, 706, 1253

Homan, D. C., Lister, M. L., Kovalev, Y. Y., et al. 2015, ApJ, 798, 134
Hovatta, T., Valtaoja, E., Tornikoski, M., & Lähteenmäki, A. 2009, A&A, 494, 527
Ikejiri, Y., Uemura, M., Sasada, M., et al. 2011, PASJ, 63, 639
Jackson, N., & Browne, I. W. A. 1991, MNRAS, 250, 414
Jorstad, S. G., Marscher, A. P., Lister, M. L., et al. 2005, AJ, 130, 1418
Jorstad, S. G., Marscher, A. P., Larionov, V. M., et al. 2010, ApJ, 715, 362
Kaspi, S., & Netzer, H. 1999, ApJ, 524, 71
Katarzyński, K., & Ghisellini, G. 2007, A&A, 463, 529
Kneiske, T. M., & Dole, H. 2010, A&A, 515, A19
Lähteenmäki, A., & Valtaoja, E. 1999, ApJ, 521, 493
Li, Z.-Y., Chiueh, T., & Begelman, M. C. 1992, ApJ, 394, 459
Lister, M. L., Cohen, M. H., Homan, D. C., et al. 2009, AJ, 138, 1874
Lister, M. L., Aller, M. F., Aller, H. D., et al. 2013, AJ, 146, 120
Liu, H. T., & Bai, J. M. 2006, ApJ, 653, 1089
Mattox, J. R., Bertsch, D. L., Chiang, J., et al. 1993, ApJ, 410, 609
Ogle, P. M., Wehrle, A. E., Balonek, T., & Gurwell, M. A. 2011, ApJS, 195, 19
Pian, E., Falomo, R., & Treves, A. 2005, MNRAS, 361, 919
Pian, E., Foschini, L., Beckmann, V., et al. 2006, A&A, 449, L21
Piner, B. G., Pushkarev, A. B., Kovalev, Y. Y., et al. 2012, ApJ, 758, 84
Poutanen, J., & Stern, B. 2010, ApJ, 717, L118
Qian, S.-J., Britzen, S., Witzel, A., et al. 2014, RAA (Research in Astronomy and Astrophysics), 14, 249
Qian, S. J., Witzel, A., Krichbaum, T., et al. 1992, Chin. Astron. Astrophys. 16, 137 (Translation of Acta Astron. Sin., 32, 4, 1991, 369)
Qian, S.-J., Kudryavtseva, N. A., Britzen, S., et al. 2007, ChJAA (Chin. J. Astron. Astrophys.), 7, 364
Raiteri, C. M., Villata, M., Larionov, V. M., et al. 2007, A&A, 473, 819
Raiteri, C. M., Villata, M., Larionov, V. M., et al. 2008a, A&A, 491, 755
Raiteri, C. M., Villata, M., Chen, W. P., et al. 2008b, A&A, 485, L17
Raiteri, C. M., Villata, M., Aller, M. F., et al. 2011, A&A, 534, A87
Savolainen, T., Homan, D. C., Hovatta, T., et al. 2010, A&A, 512, A24
Shakura, N. I., & Sunyaev, R. A. 1973, A&A, 24, 337
Sikora, M., Begelman, M. C., & Rees, M. J. 1994, ApJ, 421, 153
Stern, B. E., & Poutanen, J. 2011, MNRAS, 417, L11
Tavecchio, F., Ghisellini, G., Bonnoli, G., & Ghirlanda, G. 2010, MNRAS, 405, L94
Tavecchio, F., Maraschi, L., Ghisellini, G., et al. 2002, ApJ, 575, 137
Transtrum, M. K., & Sethna, J. P. 2012, arXiv:1201.5885
Vercellone, S., Chen, A. W., Giuliani, A., et al. 2008, ApJ, 676, L13
Villata, M., Raiteri, C. M., Balonek, T. J., et al. 2006, A&A, 453, 817
Villata, M., Raiteri, C. M., Aller, M. F., et al. 2007, A&A, 464, L5
Vlahakis, N., & Königl, A. 2004, ApJ, 605, 656
Wills, B. J., Thompson, K. L., Han, M., et al. 1995, ApJ, 447, 139
Xiang, Y., & Dai, B.-Z. 2007, PASJ, 59, 1061
Yan, D., Zeng, H., & Zhang, L. 2012, PASJ, 64, 80
Yan, D.-H., Fan, Z.-H., Zhou, Y., & Dai, B.-Z. 2013, RAA (Research in Astronomy and Astrophysics), 13, 411
Yang, J., Wang, J., Dai, B., & Gao, X. 2009, PASJ, 61, 1153
Zhang, L. Z., Fan, J.-H., & Cheng, K.-S. 2002, PASJ, 54, 159